Surface Phonon-Polaritons in Slabs of Ternary Mixed Crystals*

Bao Jin and Liang Xixia†

(*Department of Physics, Inner Mongolia University, Hohhot* 010021, *China*)

Abstract: Surface phonon-polaritons in slabs of polar ternary mixed crystals are investigated with the modified random-element-isodisplacement model and the Born-Huang approximation, based on Maxwell's equations with the usual boundary conditions. The numerical results of the surface phonon-polariton frequencies as functions of the wave-vector and thickness for slabs of ternary mixed crystals $Al_xGa_{1-x}As$, $Zn_xCd_{1-x}S$, and $Ga_xIn_{1-x}N$ are obtained and discussed. It is shown that there are four branches of surface phonon-polaritons in slab systems. The "two-mode" and "one-mode" behaviors of surface phonon-polaritons are also shown in their dispersion curves.

Key words: surface phonon-polaritons; ternary mixed crystals; slab of semiconductor
PACC: 7136; 6320; 7320M
CLC number: O471.3 **Document code**: A **Article ID**: 0253-4177(2007)12-1895-07

1 Introduction

Artificial layered materials, such as slabs, quantum wells, and superlattices have been attracting the attention of scientists with their development and applications. The study of the properties of surface phonon-polaritons associated with lattice vibrations localized near the surface coupled to electromagnetic waves is an interested topic experimentally and theoretically[1~8]. This kind of important excitations was first observed experimentally by Raman scattering and attenuated total reflection (ATR) in some slab materials and semi-infinite systems[3,4]. Later, the surface phonon-polaritons in layered systems, such as bilayer systems[5], heterostructures[6], and superlattices [7] were studied. Recently, the technique of scattering-type scanning near-field optical microscopy (s-SNOM) has been used to study mid-infrared surface phonon-polaritons propagation on bulk systems[8].

Ternary mixed crystals (TMCs) have been extensively studied due to their applications in electronic and optoelectronic devices[9~11]. There are two sets of longitudinal-transverse optical (LO-TO) phonon modes instead of one set of phonon modes in the binary crystals[9,12]. On the basis of the characteristics of the modes, the lattice vibrations of polar TMCs exhibit "one-mode" and "two-mode" behaviors. Therefore, the phonon-polaritons localized near the surfaces of slabs of TMCs, formed by a strong coupling of light and surface optical phonons, will have different properties compared to the phonon-polaritons in bulk TMCs systems and slabs of binary materials.

The surface phonon-polaritons were already shown to have applications for some photonic devices owing to the different material properties they offer, such as high temperature stability and anisotropic surface polariton properties[2,13]. The slabs of TMCs in some modulated semiconductor systems can cause new vibrational and optical properties, as well as the polariton characteristics in the systems and their applications may extend to devices[14~16]. The surface phonon-polaritons in slabs of polar binary materials are extensively investigated. However, to the best of our knowledge, the theoretical and experimental studies of the surface phonon-polaritons in slabs of polar TMCs have rarely been reported yet.

In this paper we study surface phonon-polaritons in slabs of TMCs on the basis of the random-element-isodisplacement (REI) model[12] and Born-Huang approximation[17]. The frequencies of the surface phonon-polaritons are calculated nu-

* Project supported by the Specialized Research Fund for the Doctoral Program of Higher Education of China (No. 20040126003) and the Natural Science Foundation of Inner Mongol of China (No. 200408020101)
† Corresponding author. Email: xxliang@imu.edu.cn
Received 17 June 2007

merically for several typical TMC slabs. The dispersion characteristics and their thickness dependences are discussed in detail.

2 Surface phonon-polaritons in slabs of TMCs

Consider a slab of polar TMC $A_xB_{1-x}C$ occupying the space of $|z| \leqslant d$. A surface phonon-polariton propagates along the surface of the slab with the two-dimensional wave vector $\boldsymbol{k}_{\parallel}$. For convenience, we choose the wave vector $\boldsymbol{k}_{\parallel}$ along the x direction, i.e. $k_x = k_{\parallel}$ and $k_y = 0$, without loss of generality. In the present work, we focus our attention on the surface polaritons of transverse magnetic (TM) character. The electric field $\boldsymbol{E}$ lies in the x-z plane and the magnetic field $\boldsymbol{H}$ is along the y-axis. Mills and Maradudin have investigated the polaritons in films of binary crystal materials and obtained surface modes of phonon-polaritons[18]. Here we extend their theory to the case of slabs of TMC systems. To describe the solutions localized in the vicinity of the surface of the material, the field $\boldsymbol{E}$ is chosen in the following form:

$$\boldsymbol{E} = \boldsymbol{E}(z)\exp(\mathrm{i}k_{\parallel}x - \mathrm{i}\omega t) \tag{1}$$

where

$$E(z) = \begin{cases} A^{(1)}\exp(-\kappa_1 z), & z > d \\ B^{(1)}\exp(\kappa_2 z) + B^{(2)}\exp(-\kappa_2 z), & -d < z < d \\ C^{(1)}\exp(\kappa_1 z), & z < -d \end{cases} \tag{1a}$$

which decays exponentially to zero as $z \to \pm\infty$. In Eq. (1a) κ_1 and κ_2 are respectively the decay constants of the surface waves in the vacuum and the slab of the TMC material. Both are real and positive to keep the waves decaying as they depart from the surface. They are determined by

$$\kappa_i^2 = k_{\parallel}^2 - \varepsilon_i(\omega)\omega^2/c^2, \quad i = 1,2 \tag{2}$$

Using the continuity boundary condition, the relation between the dielectric functions of the media "1" and "2" is obtained as

$$\varepsilon_2(\omega)[\exp(-\kappa_2 d) \pm \exp(\kappa_2 d)]/\kappa_2 = \varepsilon_1[\exp(-\kappa_2 d) \mp \exp(\kappa_2 d)]/\kappa_1 \tag{3}$$

Noting that the medium "1" is a vacuum and $\varepsilon_1 = 1$, we finally have the following equation:

$$\varepsilon(\omega) = \frac{\kappa_2}{\kappa_1}\left[\frac{\exp(-\kappa_2 d) \mp \exp(\kappa_2 d)}{\exp(-\kappa_2 d) \pm \exp(\kappa_2 d)}\right] \tag{4}$$

where the upper one of the plus and minus signs in Eq. (4) is subjected to the higher branch of frequencies in the slab and the down sign to the lower-frequency one. The corresponding dielectric functions are respectively written as

$$\varepsilon(\omega) = -(\kappa_2/\kappa_1)\tanh(\kappa_2 d) \tag{5}$$

for the high-frequency branch and

$$\varepsilon(\omega) = -(\kappa_2/\kappa_1)\coth(\kappa_2 d) \tag{6}$$

for the low-frequency branch. It is evident from Eqs. (5) and (6) that the surface polariton waves can exist only in the region where the dielectric function of the slab of TMC is negative, i.e. $\varepsilon(\omega) < 0$.

The dielectric function $\varepsilon(\omega)$ in the TMC can be obtained by using the modified random-element-isodisplacement (MREI) model[12] and Born-Huang-like equations[17] describing the lattice vibrations of the TMC systems.

The Born-Huang-like equation group for the TMC can be written as

$$\ddot{\boldsymbol{W}}_1 = b_{11}\boldsymbol{W}_1 + b_{12}\boldsymbol{W}_2 + b_{13}\boldsymbol{E} \tag{7}$$

$$\ddot{\boldsymbol{W}}_2 = b_{21}\boldsymbol{W}_1 + b_{22}\boldsymbol{W}_2 + b_{23}\boldsymbol{E} \tag{8}$$

$$\boldsymbol{P} = b_{31}\boldsymbol{W}_1 + b_{32}\boldsymbol{W}_2 + b_{33}\boldsymbol{E} \tag{9}$$

In Eqs. (7) ~ (9), $\boldsymbol{W}_1 = \mu_1^{1/2}\boldsymbol{s}_1$ and $\boldsymbol{W}_2 = \mu_2^{1/2}\boldsymbol{s}_2$, where $\boldsymbol{s}_1 = (\boldsymbol{u}_A - \boldsymbol{u}_C)$ and $\boldsymbol{s}_2 = (\boldsymbol{u}_B - \boldsymbol{u}_C)$ are respectively the relative displacements of the A-C ion and B-C ion pairs, and μ_1 and μ_2 are the corresponding reduced masses. u_A, u_B, and u_C are respectively the displacements of the ions A, B, and C. $\boldsymbol{E}$ is the macroscopic electric field and $\boldsymbol{P}$ is the polarization. The dynamical coefficient b_{ij} ($i, j = 1,2,3$) has been determined previously[19,20]. Here we do not show the details and, instead, use the results directly.

$$b_{11} = -\omega_{TA}^2\eta_A\frac{M_C + M_A x}{M_C + M_A} + \omega_{TA}\left[\omega_{TA}\kappa_A\sigma_A\frac{M_C + M_A x}{M_C + M_A} + \omega_{TB}(\kappa_A\kappa_B\sigma_A\sigma_B\mu_B/\mu_A)^{1/2}\frac{M_A(1-x)}{M_C + M_A}\right]xa(x) \tag{10}$$

$$b_{12} = -\omega_{TB}^2\eta_B\frac{M_B(1-x)}{M_C + M_B}(\mu_A/\mu_B)^{1/2} + \omega_{TB}\left[\omega_{TB}\kappa_B\sigma_B(\mu_B/\mu_A)^{1/2}\frac{M_A(1-x)}{M_C + M_A} + \omega_{TA}(\kappa_A\kappa_B\sigma_A\sigma_B)^{1/2}\frac{M_C + M_A x}{M_C + M_A}\right](1-x)a(x) \tag{11}$$

$$b_{13} = \left[\omega_{TA}(\kappa_A\sigma_A)^{1/2}\frac{M_C + M_A x}{M_C + M_A} + \omega_{TB}(\kappa_B\sigma_B\mu_B/\mu_A)^{1/2}\frac{M_A(1-x)}{M_C + M_A}\right]\varepsilon_0^{1/2}a(x) \tag{12}$$

$$b_{21} = -\omega_{TA}^2\eta_A\frac{M_A x}{M_C+M_A}(\mu_B/\mu_A)^{1/2} + \omega_{TA}\left[\omega_{TA}\kappa_A\sigma_A(\mu_A/\mu_B)^{1/2}\frac{M_B x}{M_C+M_B} + \omega_{TB}(\kappa_A\kappa_B\sigma_A\sigma_B)^{1/2}\frac{M_C+M_B(1-x)}{M_C+M_B}\right]xa(x) \tag{13}$$

$$b_{22} = -\omega_{TB}^2\eta_B\frac{M_C+M_B(1-x)}{M_C+M_B} + \omega_{TB}\left[\omega_{TB}\kappa_B\sigma_B\frac{M_C+M_B(1-x)}{M_C+M_B} + \omega_{TA}(\kappa_A\kappa_B\sigma_A\sigma_B\mu_A/\mu_B)^{1/2}\frac{M_B x}{M_C+M_B}\right](1-x)a(x) \tag{14}$$

$$b_{23} = \left[\omega_{TB}(\kappa_B\sigma_B)^{1/2}\frac{M_C+M_B(1-x)}{M_C+M_B} + \omega_{TA}(\kappa_B\sigma_A\mu_A/\mu_B)^{1/2}\frac{M_B x}{M_C+M_B}\right]\varepsilon_0^{1/2}a(x) \tag{15}$$

$$b_{31} = \omega_{TA}(\kappa_A\sigma_A)^{1/2}\varepsilon_0^{1/2}xa(x) \tag{16}$$

$$b_{32} = \omega_{TB}(\kappa_B\sigma_B)^{1/2}\varepsilon_0^{1/2}(1-x)a(x) \tag{17}$$

$$b_{33} = \varepsilon_0[a(x)-3] \tag{18}$$

where $a(x)=3/[1-\gamma_A\sigma_A x-\gamma_B\sigma_B(1-x)]$, $\sigma_l \equiv v_l/v$, $\gamma_l = \frac{\varepsilon_{\infty l}-1}{\varepsilon_{\infty l}+2}$, $\kappa_l = \frac{\varepsilon_{sl}-\varepsilon_{\infty l}}{(\varepsilon_{\infty l}+2)^2}$, $\eta_l = \frac{\varepsilon_{sl}+2}{\varepsilon_{\infty l}+2}$, $(l = A,B)$.

In the above equations, ε_{sl} and $\varepsilon_{\infty l}$ are respectively the static and optical dielectric constants of the end-member materials (AC for $l=$ A and BC for $l=$ B). M_A, M_B, and M_C are respectively the masses of ions A, B, and C.

$$\mu_A = \frac{M_C M_A}{M_C+M_A}, \text{ and } \mu_B = \frac{M_C M_B}{M_C+M_B}.$$

ω_{TA} and ω_{TB} are respectively the TO-phonon frequencies of materials AC and BC.

Let us write the solution of Eqs. (7)～(9) in the following form:

$$\boldsymbol{W},\boldsymbol{P},\boldsymbol{E} \propto \exp[i(\boldsymbol{k}\cdot\boldsymbol{r}-\omega t)] \tag{19}$$

where ω and $\boldsymbol{k}$ are respectively the frequency and wave-vector of the phonon-polaritons. Inserting the solutions from Eq. (19) into Eqs. (7)～(9), one can obtain the following relation between the macroscopic electric field $\boldsymbol{E}$ and the polarization $\boldsymbol{P}$:

$$\boldsymbol{P} = \left\{b_{31}\left[\frac{b_{23}b_{12}-b_{13}(b_{22}+\omega^2)}{(b_{11}+\omega^2)(b_{22}+\omega^2)-b_{12}b_{21}}\right] + b_{32}\left[\frac{b_{13}b_{21}-b_{23}(b_{11}+\omega^2)}{(b_{11}+\omega^2)(b_{22}+\omega^2)-b_{12}b_{21}}\right] + b_{33}\right\}\boldsymbol{E} \tag{20}$$

The dielectric function of the TMC then can be written as

$$\varepsilon(\omega) = 1+\chi(\omega)/\varepsilon_0 \tag{21}$$

where

$$\chi(\omega) = \left\{b_{31}\left[\frac{b_{23}b_{12}-b_{13}(b_{22}+\omega^2)}{(b_{11}+\omega^2)(b_{22}+\omega^2)-b_{12}b_{21}}\right] + b_{32}\left[\frac{b_{13}b_{21}-b_{23}(b_{11}+\omega^2)}{(b_{11}+\omega^2)(b_{22}+\omega^2)-b_{12}b_{21}}\right] + b_{33}\right\} \tag{22}$$

Equations (5) and (6) can be solved numerically and give the frequencies of the surface phonon-polaritons as functions of the 2D wave vector $k_\parallel$ as well as the composition x by using the expressions of Eqs. (21) and (22) for the dielectric function $\varepsilon(\omega)$ in the TMC.

3 Numerical results and discuss

The numerical calculations for the frequencies of surface phonon-polaritons for several slabs of TMCs of III-V, II-VI compound semiconductors with various composition x have been performed. As examples, the calculated results for the slabs of the TMCs $Al_xGa_{1-x}As$, $Zn_xCd_{1-x}S$, and $Ga_xIn_{1-x}N$ are illustrated in Figs. 1～3. In the calculations the composition x is chosen successively as 0, 0.35, 1; 0, 0.5, 1; and 0, 0.69, 1 for the three systems. The parameters used are listed in Table 1.

The dispersion curves of the surface phonon-polaritons in slabs of several TMC materials are plotted in Fig. 1. The dispersion characteristic of surface phonon-polaritons in TMC slabs is quite different from that in bulk and semi-infinite materials and slabs of binary systems. As was expected, the dispersion curves degenerate respectively to those of the corresponding binary systems GaAs, CdS, and InN or AlAs, ZnS, and GaN when

Table 1　Optical phonon energies, dielectric constants, effective masses of electrons, and the lattice constants for binary materials　Energy is measured in meV, m in the electron rest mass, and the lattice constants in nm.

Material	$\hbar\omega_{TO}$	$\hbar\omega_{LO}$	ε_0	ε_∞	m	M /a.u.		a
AlAs[a]	44.88	50.09	10.06	8.16	0.150	26.99	74.92	0.5660[c]
GaAs[a]	33.29	36.25	13.18	10.89	0.067	69.72	74.92	0.56419[c]
ZnS[b]	34.65	44.00	8.00	5.14	0.280	65.38	32.06	0.5410[c]
CdS[b]	30.25	38.24	8.42	5.27	0.155	112.4	32.06	0.5825[c]
GaN[d]	69.43	91.87	9.5	5.35	0.20	69.72	14.01	0.5185[c]
InN[d]	59.27	86.05	9.3	7.72	0.11	114.8	14.01	0.5760[c]

[a] Reference [21]　[b] Reference [22]　[c] Reference [23]　[d] Reference [11]

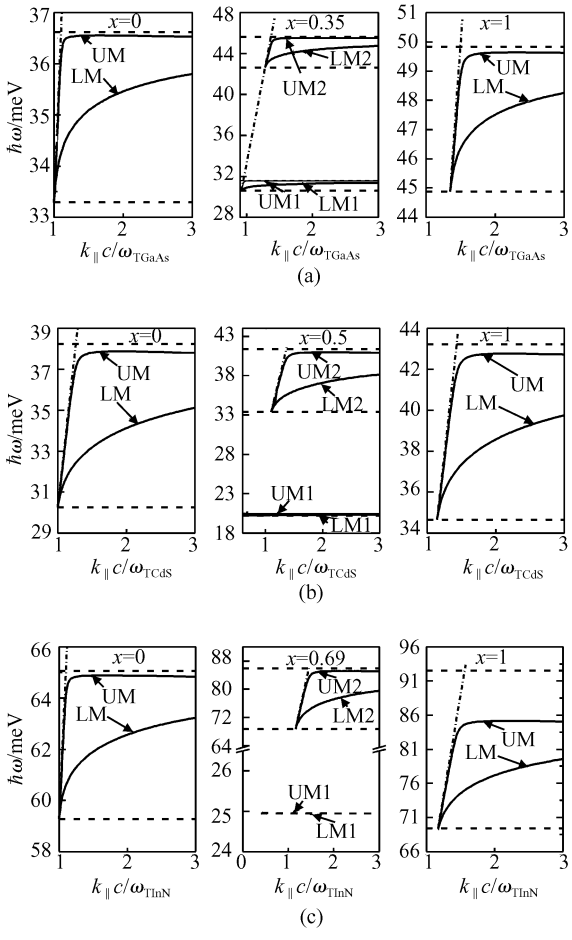

Fig. 1 Energies of the surface phonon-polaritons (solid) as functions of the wave-vector $k_{\parallel}$ for slabs of TMCs system for $Al_xGa_{1-x}As$ (a), $Zn_xCd_{1-x}S$ (b), and $Ga_xIn_{1-x}N$ (c) The dimensionless wave-vectors $k_{\parallel}c/\omega_{TGaAs}$, $k_{\parallel}c/\omega_{TCdS}$, and $k_{\parallel}c/\omega_{TInN}$ are used, where ω_{TGaAs}, ω_{TCdS}, and ω_{TInN} are the frequencies of TO phonons for GaAs, CdS, and InN and c the velocity of light. Energies of the long-wavelength TO and LO phonons (long-dashed) and the "photons" (dashed-dotted) are also plotted for comparison.

$x = 0$ or 1, where there are only two branches of surface phonon-polaritons, both of which are in the forbidden band for the bulk phonon-polaritons between ω_{TO} and ω_{LO} of binary crystals. The higher-frequency modes in two surface phonon-polariton branches are antisymmetric, and we called them the upper modes (UM). The symmetric modes in the lower-frequency branch are called the lower modes (LM).

When the composition x is neither 0 nor 1, the dispersion curves display their TMC characteristic. Different from the binary systems, there are generally four branches of surface phonon-polariton frequencies divided into two groups, being situated respectively in two forbidden bands of bulk phonon-polaritons between the LO and TO frequencies subject respectively to the BC- and AC-like LO-TO pairs in TMC $A_xB_{1-x}C$. Every group in forbidden bands includes two branches of surface phonon-polariton frequencies related to the antisymmetric and symmetric modes, respectively. However, the four polariton frequencies may not all be observed easily because their forbidden bands have different widths so that the "two-mode" and "one-mode" behaviors also appear in the dispersion curves of surface phonon-polaritons in TMC slabs.

Two mode behavior of the surface phonon-polaritons in the slab of TMC $Al_{0.35}Ga_{0.65}As$ is clearly seen in Fig. 1(a). Two forbidden bands of bulk phonon-polaritons in $Al_{0.35}Ga_{0.65}As$ are wider so that four branches of surface phonon-polaritons in the bands can be considerably separated from each other by frequencies. The upper pair of surface phonon-polariton frequencies (UM2-LM2) lies in the upper forbidden band between the AlAs-like LO and TO frequencies, and the lower pair (UM1-LM1) in the GaAs-like forbidden band. Two pairs of curves first start respectively from the frequencies of the higher and lower branches of TO phonons in the bulk TMC $A_xB_{1-x}C$ at the wave vectors $k_{\parallel}\to\omega_{2T}/c$ and ω_{1T}/c, and then each pair separates quickly into two branches(UM and LM). Finally, they tend to two SO-phonon frequencies, ω_{2S} (AlAs-like) and ω_{1S} (GaAs-like), as $k_{\parallel}\to\infty$. The width of the forbidden band of the GaAs-like modes (the lower) is only around 1meV, which is one third of that of AlAs-like modes (about 3 meV) for $Al_{0.35}Ga_{0.65}As$. Therefore one can infer that the upper pair (UM2-LM2) of the surface phonon-polaritons for the slab of $Al_{0.35}Ga_{0.65}As$ is easily observed, but the lower is slightly difficult.

The "one-mode" behavior characteristic of the surface phonon-polaritons is shown in Figs. 1 (b) and (c) for the slabs of TMCs $Zn_{0.5}Cd_{0.5}S$ and $Ga_{0.69}In_{0.31}N$. Figures 1 (b) and (c) show that only one pair of surface phonon-polaritons (UM2-LM2) is observable, which lies in the wider upper forbidden bands between the ZnS-like and GaN-like LO and TO frequencies with the widths around 8 and 17meV, respectively. Therefore the

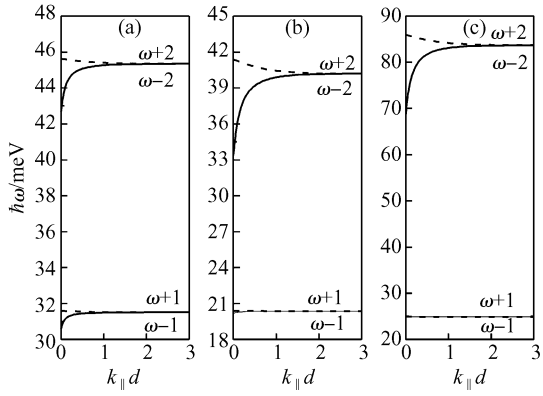

Fig. 2　Energies of the antisymmetric (long dashed lines) and symmetric (solid lines) surface phonon modes as functions of the wave-vector for the slabs of $Al_{0.35}Ga_{0.65}As$ (a), $Zn_{0.5}Cd_{0.5}S$ (b), and $Ga_{0.69}In_{0.31}N$ (c)

surface modes (UM2-LM2) in the upper band can be considerably separated from each other by frequencies and observed experimentally. In contrast, the curves of the lower pair of surface polaritons (UM1-LM1) are nearly two horizontal lines close to each other, whose frequencies fall in the lower bulk-polariton propagated bands, so that it is difficult to observe them independently.

The "two-mode" and "one-mode" mode behaviors of surface modes in TMC slabs can also be understood by calculating the SO phonon frequencies as functions of the wave vector. Letting $\kappa_1 = \kappa_2 = k_\parallel$ in Eq. (4), we can obtain the following equation satisfied by SO phonon modes in a TMC slab:

$$\varepsilon(\omega) = \left[\frac{\exp(-k_\parallel d) \mp \exp(k_\parallel d)}{\exp(-k_\parallel d) \pm \exp(k_\parallel d)}\right] \quad (22)$$

Solving numerically Eq. (22) with Eqs. (20) and (21), we have obtained the SO phonon frequencies as functions of the dimensionless wave vector $k_\parallel d$ for the slabs of $Al_xGa_{1-x}As$, $Zn_xCd_{1-x}S$, and $Ga_xIn_{1-x}N$ and the results are illustrated in Fig. 2.

For the slab of "two-mode" behavior TMC $Al_xGa_{1-x}As$ in Fig. 2(a), two pairs of observable SO-phonon frequencies, $\omega_{+1} - \omega_{-1}$ and $\omega_{+2} - \omega_{-2}$, lie between the LO and TO modes respectively subject to the GaAs-like (the lower) and AlAs-like (the higher) LO—TO pairs. Two frequency pairs start respectively from the frequencies of long-wavelength LO-phonons (ω_{2L}) and TO-phonon (ω_{2T}) for the upper pair and ω_{1L} and ω_{1T} for lower pair at $k_\parallel \to 0$. As the wave-vector $k_\parallel$ increases, the two frequencies of each pair converge to a limit that is the same as in the semi-infinite system (ω_{1S} for the GaAs-like or ω_{2S} for another) at $k_\parallel d \to \infty$.

Table 2　Calculated bulk and surface optical phonon energies for several ternary mixed crystals　Energy is measured in meV.

Material	$\hbar\omega_{1S}$	$\hbar\omega_{2S}$	$\hbar\omega_{1L}$	$\hbar\omega_{1T}$	$\hbar\omega_{2L}$	$\hbar\omega_{2T}$
$Al_{0.35}Ga_{0.65}As$	31.52	45.34	31.59	30.59	45.62	42.64
$Zn_{0.5}Cd_{0.5}S$	20.37	40.19	20.39	20.18	41.38	33.36
$Ga_{0.69}In_{0.31}N$	24.95	83.70	24.97	24.94	85.96	68.72

On the other hand, the "one-mode" behavior is shown in the curves of SO-phonon frequencies for $Zn_xCd_{1-x}S$ and $Ga_xIn_{1-x}N$ in Figs. 2(b) and (c). The mode pair with the higher frequencies ω_{+2} and ω_{-2} is dominant in this kind of system. Their dispersion curves are similar to that in the $Al_xGa_{1-x}As$ system of Fig. 2(a). However, the other two branches with lower frequencies ($\omega_{+1} - \omega_{-1}$ pair) degenerate into a horizontal line and are difficult to observe because of the very weak oscillator strength.

The above-mentioned frequencies of TO and LO phonons as well as SO phonons in semi-infinite materials were calculated but we do not discuss them in detail here. Our calculated results for the above-mentioned systems are listed in Table 2 for reference.

Equations (5) and (6) indicate that the frequencies of the surface phonon-polaritons in a TMC slab also depend, not only on the wave vector, but also on the slab width. To understand the characteristic of the dependence of surface phonon-polariton modes on the slab widths, we plot the dispersion curves of surface phonon-polaritons for the slabs of TMC $Al_xGa_{1-x}As$, $Zn_xCd_{1-x}S$, and $Ga_xIn_{1-x}N$ with different thicknesses in Fig. 3. Two groups of surface polariton branches are plotted for the two-mode behavior system (Fig. 3 (a)), but only one group of branches for the one-mode behavior systems (Figs. 3 (b), (c)).

The two branches of polariton frequencies in a forbidden band for bulk polaritons separate considerably at the long-wavelengths and move closer as the wave-vector increases. On the other hand, the interval between the higher and lower frequency branches varies obviously with the thickness of the slab. As the slab is thinner, the separation of the two frequency branches is visible, espe-

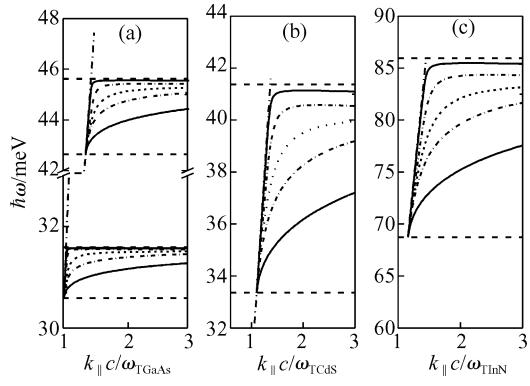

Fig. 3 Energies of the surface phonon-polaritons for slab half-thicknesses of $d = 10^2$ nm (solid), 10^3 nm (short dashed-dotted) and 10^4 nm (short-dashed) as functions of the wave-vector $k_{\parallel}$ in slabs of TMC systems of $Al_{0.35}Ga_{0.65}As$ (a), $Zn_{0.5}Cd_{0.5}S$ (b), and $Ga_{0.69}In_{0.31}N$ (c) Energies of the long-wavelength TO and LO phonons (long-dashed) and the "photons" (dashed-dotted) are also plotted for comparison.

cially for the small wave-vectors, and the higher one is near the edge of the bulk-polariton forbidden band, i. e. the LO frequency. The splitting of the two branches of surface phonon-polariton curves in a forbidden band for bulk polaritons decreases with increasing the thickness of the slab. Figure 4 shows the splitting energies of the two branches of surface phonon-polaritons as functions of the half-thickness d in the slabs of TMCs for the same systems. It is more clearly seen from the figure that the splitting is reduced quickly as the slab thickness increases, and falls to zero as $d \to \infty$. The two branches of slab surface phonon-polariton modes degenerate to one branch corresponding "semi-infinite" TMCs.

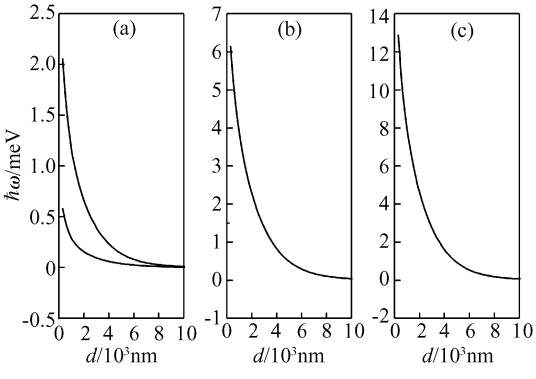

Fig. 4 Splitting energies of the surface phonon-polaritons as functions of the half-thickness d in the slabs of TMCs for $Al_{0.35}Ga_{0.65}As$ (a), $Zn_{0.5}Cd_{0.5}S$ (b), and $Ga_{0.69}In_{0.31}N$ (c) for $k_{\parallel} = 2$ The wave-vector $k_{\parallel}$ is measured in $\omega_{\mathrm{TGaAs}}/c$, ω_{TCdS}/c, and ω_{TInN}/c, respectively.

The special properties of column III-nitride (III-N) compound semiconductors attract many scientists due to their potential developmental prospects. For example, III-N compound TMCs get much stronger electron-phonon coupling and more obvious nonlinearity than those in other III-V compounds and even II-VI compounds[20]. As expected, novel characteristics also appear for the surface phonon-polaritons in III-N TMC slabs. The III-N TMC $Ga_{0.69}In_{0.31}N$ expresses clearly their "one-mode" behavior and has a wide interval between the frequencies of two surface polariton modes in a forbidden band for bulk-modes. Figure 3 shows that the splitting of two frequency curves of the main branches of surface polaritons in $Ga_{0.69}In_{0.31}N$ slab is up to 14meV, which is much larger than that in other III-V compound systems (around 2meV For $Al_{0.35}Ga_{0.65}As$) and even in a II-V compound $Zn_{0.5}Cd_{0.5}S$ system (around 6meV). Therefore the surface phonon-polaritons in III-N TMC slabs are easily observed experimentally.

4 Conclusion

We have investigated theoretically the surface phonon-polaritons of slabs of TMCs in the MREI model and the Born-Huang approximation, based on the Maxwell's equations with the usual boundary conditions. The frequencies of the surface phonon-polaritons were calculated. The numerical results for slabs of TMCs $Al_xGa_{1-x}As$, $Zn_xCd_{1-x}S$, and $Ga_xIn_{1-x}N$ show that there are four branches of surface phonon-polaritons in the two forbidden bands of bulk phonon-polaritons. The "two-mode" and "one-mode" behaviors of TMCs are also shown in the dispersion curves of surface phonon-polaritons.

We have also considered the III-N compound $Ga_xIn_{1-x}N$ slabs in NaCl structure to calculate its dispersion curves of surface phonon-polaritons. The results show that the surface phonon-polaritons are easily observed because of the wider forbidden band of bulk phonon-polaritons. It should be pointed out that the III-N compounds are usually grown in a wurtzite structure, which is not of a cubic lattice. More accurate calculations for III-N TMC slabs should take the non-cubic lattice into account and will be the subject of future investigations.

References

[1] Chen D Z A, Narayanaswamy A, Chen G. Surface phonon-polariton mediated thermal conductivity enhancement of amorphous thin films. Phys Rev B, 2005, 72(15): 155435

[2] Anderson M S. Enhanced infrared absorption with dielectric nanoparticles. Appl Phys Lett, 2003, 83(14): 2964

[3] Marschall N, Fischer B. Dispersion of surface polaritons in GaP. Phys Rev Lett, 1972, 28(13): 811

[4] Torii K, Koga T, Sota T, et al. An attenuated-total- reflection study on the surface phonon-polariton in GaN. J Phys: Condens Matter, 2000, 12(31): 7041

[5] Wendler L, Jäger E. Phonon-polaritons in bilayer systems. Phys Status Solidi B, 1983, 120(1): 235

[6] Nakayama M, Ishida M, Sano N. Raman scattering by interface-phonon polaritons in a GaAs/AlAs heterostructure. Phys Rev B, 1988, 38(9): 6348

[7] Nkoma J S. Phonon polariton modes in semiconductor superlattices. Solid State Commun, 1987, 64(11): 1383

[8] Huber A, Ocelic N, Kazantsev D, et al. Near-field imaging of mid-infrared surface phonon polariton propagation. Appl Phys Lett, 2005, 87(8): 081103

[9] Taylor D W. Optical properties of mixed crystals. Elliot R J, Ipatova I P, ed. Amsterdam: North-Holland, 1988

[10] Wu Jian. Long-wavelength optical phonon spectra of mixed crystals. Chinese Journal of Semiconductors, 1980, 1(4): 267 (in Chinese) [吴汲安. 混晶的长波长光学声子谱. 半导体学报, 1980, 1(4): 267]

[11] Yu S, Kim K W, Bergman L, et al. Long-wavelength optical phonons in ternary nitride-based crystals. Phys Rev B, 1998, 58(23): 15283

[12] Chang I F, Mitra S S. Long wavelength optical phonons in mixed crystals. Adv Phys, 1971, 20(85): 359

[13] Shvets G. Photonic approach to making a material with a negative index of refraction. Phys Rev B, 2003, 67(3): 035109

[14] Woo T, Kim J H, Kim T W, et al. Optical and electronic properties in $(In_{0.53}Ga_{0.47}As)_{1-z}/(In_{0.52}Al_{0.48}As)_z$ digital alloys. Phys Rev B, 2005, 72(20): 205320

[15] Yao Shude, Wu Mingfang, Chen Shouyuan, et al. Rutherford backscattering and channeling study of heteroeptiaxial GaN and its ternary alloy. Chinese Journal of Semiconductors, 1999, 20(1): 25 (in Chinese) [姚淑德, 吴名枋, 陈守元, 等. 异质外延 GaN 及其三元合金薄膜的 RBS/Channeling 研究. 半导体学报, 1999, 20(1): 25]

[16] Chen K Q, Wang X H, Gu B Y. Effect of structural defects consisting of ternary mixed crystals on localized interface optical modes in superlattices. Phys Rev B, 2002, 65(15): 153305

[17] Born M, Huang K. Dynamical theory of crystal lattices. New York: Oxford University Press, 1954

[18] Mills D L, Maradudin A A. Properties of surface polaritons in layered structures. Phys Rev Lett, 1973, 31(6): 372

[19] Liang X X, Yang J S. Effective-phonon approximation of polarons in ternary mixed crystal. Solid State Commun, 1996, 100(9): 629

[20] Liang X X, Ban S L. Optical vibration modes and electron-phonon interaction in ternary mixed crystals of polar semiconductors. Chin Phys, 2004, 13(1): 71

[21] Adachi S. GaAs, AlAs, and $Al_xGa_{1-x}As$ material parameters for use in research and device applications. J Appl Phys, 1985, 58(3): R1

[22] Kartheuser E. Polarons in ionic crystals and polar semiconductors. Devreese J T, ed. Amsterdam: North-Holland, 1973: 718

[23] Strite S, Morkoc H. GaN, AlN, and InN: a review. J Vac Sci Technol B, 1992, 10(4): 1237

三元混晶膜的表面声子极化激元*

包　锦　梁希侠†

（内蒙古大学物理系，呼和浩特　010021）

摘要：采用改进的无规元素孤立位移模型和波恩-黄近似，运用电磁场的麦克斯韦方程和边界条件，研究极性三元混晶膜中的表面声子极化激元. 以 $Al_xGa_{1-x}As$，$Zn_xCd_{1-x}S$ 和 $Ga_xIn_{1-x}N$ 膜为例，获得了其中表面声子极化激元的频率作为波矢和膜厚之函数的数值结果并进行了讨论. 结果表明：在三元混晶膜中有四支表面声子极化激元，不同材料的色散曲线分别显示了混晶电磁声子模的“双模”和“单模”特征.

关键词：表面声子极化激元；三元混晶；半导体膜

PACC：7136；6320；7320M

中图分类号：O471.3　　**文献标识码**：A　　**文章编号**：0253-4177(2007)12-1895-07

* 教育部高等学校博士学科点专项基金（批准号：20040126003）和内蒙古自治区自然科学基金（批准号：200408020101）资助项目

† 通信作者. Email: xxliang@imu.edu.cn

2007-06-17 收到